Advances in Applied Mathematics and Mechanics
Adv. Appl. Math. Mech., Vol. **8**, No. 5, pp. 737-756

DOI: 10.4208/aamm.2015.m1175
October 2016

Multi-Zone Ice Accretion and Roughness Models for Aircraft Icing Numerical Simulation

Chengxiang Zhu[1,*], Chunling Zhu[2] and Tao Guo[2]

[1] *Key Laboratory of Fundamental Science for National Defense-Advanced Design Technology of Flight Vehicle, Nanjing University of Aeronautics and Astronautics, Nanjing 210016, China*
[2] *College of Aerospace Engineering, Nanjing University of Aeronautics and Astronautics, Nanjing 210016, China*

Received 27 June 2015; Accepted (in revised version) 6 September 2015

Abstract. A mathematical multi-zone ice accretion model used in the numerical simulation of icing on airfoil surface based on three water states, namely, continuous film, rivulets and beads is studied in this paper. An improved multi-zone roughness model is proposed. According to the flow state of liquid water and film flow, rivulets flow governing equations are established to calculate film mass distribution, film velocity, rivulet wetness factor and rivulet mass distribution. Force equilibrium equations of droplet are used to establish the critical conditions of water film broken into rivulets and rivulets broken into beads. The temperature conduction inside the water layer and ice layer is considered. Using the proposed model ice accretion on a NACA0012 airfoil profile with a 4° angle of attack under different icing conditions is simulated. Different ice shapes like glaze ice, mixed ice and rime ice are obtained, and the results agree well with icing wind tunnel experiment data. It can be seen that, water films are formed on the surface, and heights of the films vary with icing time and locations. This results in spatially-temporally varying surface roughness and heat transfer process, ultimately affects the ice prediction. Model simulations indicate that the process of water film formation and evolution cannot be ignored, especially under glaze ice condition.

AMS subject classifications: 76T10, 80A20

Key words: Ice accretion model, multi-zone, film, rivulets, beads, roughness height, heat transfer, temperature conduction.

1 Introduction

Because aircraft icing is a serious threat to flight safety, aircraft must have an efficient anti/de-icing system. No matter which ice protection method is used, the ice accretion

*Corresponding author.
Email: cxzhu@nuaa.edu.cn (C. X. Zhu), clzhu@nuaa.edu.cn (C. L. Zhu), guotao5134@163.com (T. Guo)

 ©2016 Global Science Press

https://doi.org/10.4208/aamm.2015.m1175 Published online by Cambridge University Press

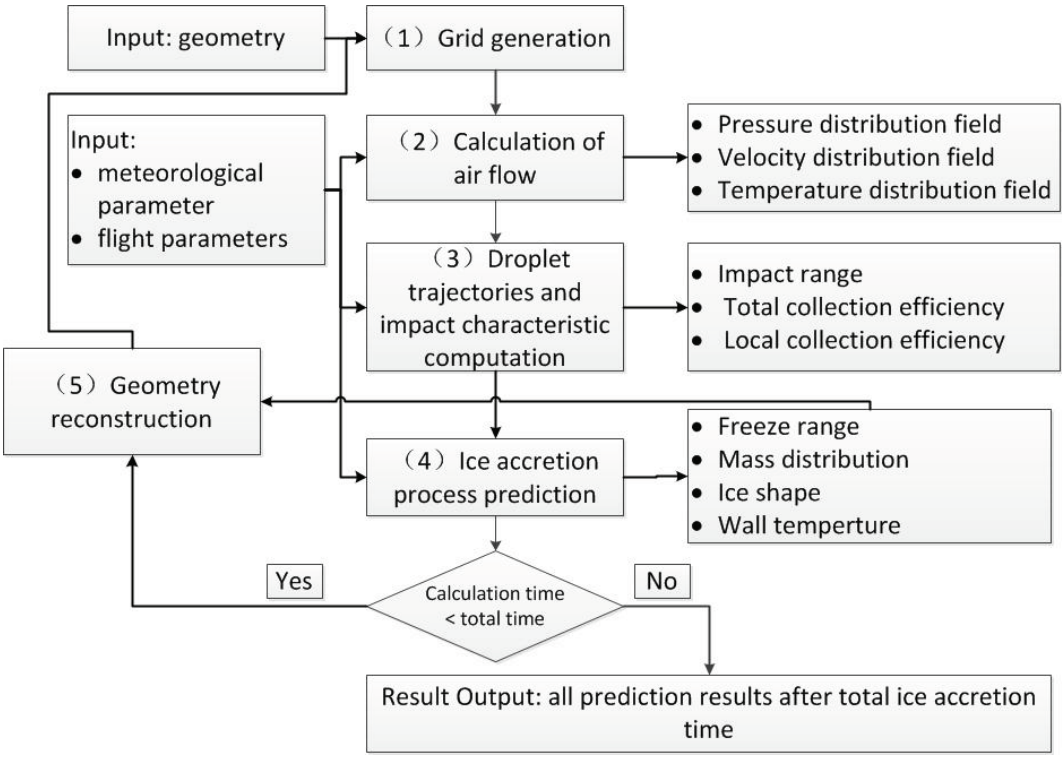


Figure 1: Calculation flow diagram of aircraft icing numerical simulation.

process must be accurately predicted to determine the structure and shape of the ice, its extension and mass distribution, which are important design basis for various ice protection systems.

In general, numerical simulation of icing consists of four modules: (1) generation of computational mesh, (2) calculation of air flow, (3) calculation of water droplet trajectories and impact characteristic, and (4) prediction of ice accretion. Since the aircraft icing is an unsteady process, the ice formed on the leading surface of a wing may change the aerodynamic configuration. Subsequently the air flow and droplet trajectories are also affected, eventually the ice accretion is also influenced. So, a new module: reconstruction of the iced airfoil geometry should be involved in the simulation. Fig. 1 shows the simulation flow chart. As the velocity and pressure of the air flow, and impact droplet mass distribution are obtained from the previous three modules, flowing process and heat and mass transfer of droplet collected by the wall will be determined in the fourth module. The icing extension, ice mass distribution and ice shape will be calculated simultaneously. To obtain accurate and reliable CFD predictions, each module is very important. This paper focuses on a new multi-zone ice accretion and surface roughness model in the fourth module to more accurately simulate the revolutionary process of impact droplet on the wall.

https://doi.org/10.4208/aamm.2015.m1175 Published online by Cambridge University Press

Since 1900s, a number of aircraft icing prediction codes/software packages have been developed, such as LEWICE [1], ONERA [2], DRA [3], CIRAMIL [4], FENSAP-ICE [5], etc. Although all these packages include the above four main modules, models used in different modules are different. The first four software packages adopt Messinger ice accretion model, which is still widely used. Messinger model combines mass and heat balance equations to determine the runback water on the surface with the hypothesis that water film is continuous and uniform. However, experiments [6–9] have shown that water droplets impinge the airfoil surface and subsequently form a thin water film at leading edge. When the environmental temperature is not low enough, droplets may not freeze immediately, and flow downstream. Due to evaporation, sublimation and freeze, the film thickness may vary in stream-wise direction. In some cases, the water film breaks down and forms rivulets and beads. Movement of droplets on the airfoil surface directly alters ice freezing scape, mass distribution and surface roughness, and further affects the heat and mass transfer process and ice shape. Therefore, when the temperature is relatively high, there is a big discrepancy between parameter values characterizing icing on the airfoil surface obtained by simulations using Messinger ice accretion model and those measured experimentally.

FENSAP-ICE employed a shallow water icing model, which established mass and energy conservation differential equations for continuous film flow on an iced surface. It took into account the effects of surface roughness in an one-equation turbulence model [10] and determined the heat transfer based on the temperature distribution near the wall. Recently, FENSAP-ICE developed a bead and rivulet model [11,12] using lagrangian model to identify the main statistical features of the stochastic process of bead nucleation, growth and coalescence under glaze ice conditions. The roughness was also simulated. But the temperature distribution in the film was not considered in the energy equation.

In this paper, a multi-zone ice accretion model is proposed to take into account movement of impinged droplets. Water film flow region, rivulets flow region and beads formation region are identified. For each region, a special spatially varied roughness model is established to predict the roughness and its effects on the heat transfer. Using the new model, ice accretion process on NACA0012 airfoil is predicted and compared to IRT experiment results under the same conditions. Simulations show that models presented in this paper may improve accuracy of model prediction of airfoil icing. Formation and development of water film and roughness on the surface should be considered in aircraft icing simulation, especially for glaze ice conditions.

Rest of this paper is organized as follows. A multi-zone ice accretion model is described in details including description of water film mathematical model, critical conditions for water film breakdown and rivulets breakdown in Section 2. A multi-zone roughness model is presented in Section 3 and heat transfer in layers and on the water-ice interface considering the effects of surface roughness is described in Section 4. Numerical methods for solving governing equations are discussed in Section 5. This is followed by the results and discussion section, which includes model validation and description of the predictive simulation.

https://doi.org/10.4208/aamm.2015.m1175 Published online by Cambridge University Press

2 Multi-zone ice accretion model

2.1 Mathematical model of water film

As droplets hit the wall, water film forms [6–9] and flows downstream driven by gravity, shear forces, surface tension, etc. Following assumptions are made based on the fact that this water film is thin and moves with low speed [10]:

- The water film on iced surface is defined as an incompressible laminar flow.
- The influence of water film on air flow is ignored.
- The influence of the impacting water droplets on water film is ignored.

As the temperature gradient is small in the film, film physical properties can be regarded as approximately constant. Then, the momentum equations of incompressible laminar flow for the continuous water film can be presented as:

$$\rho_w \frac{\partial u}{\partial t} + \rho_w \left(u \frac{\partial u}{\partial s} + v \frac{\partial u}{\partial y} \right) = -\frac{\partial p}{\partial s} + \mu \left(\frac{\partial^2 u}{\partial s^2} + \frac{\partial^2 u}{\partial y^2} \right) + \rho_w g_s, \tag{2.1a}$$

$$\rho_w \frac{\partial v}{\partial t} + \rho_w \left(u \frac{\partial v}{\partial s} + v \frac{\partial v}{\partial y} \right) = -\frac{\partial p}{\partial y} + \mu \left(\frac{\partial^2 v}{\partial s^2} + \frac{\partial^2 v}{\partial y^2} \right) + \rho_w g_y. \tag{2.1b}$$

Taking the curvilinear coordinate system based on the iced surface, which may be flat or curve, water film flowing direction is defined as $\check{s}$, and face normal direction is defined as $\check{y}$, as shown in Fig. 2, the droplet velocity in these two directions are u and v respectively. p is air pressure of the surface, ρ_w is the water density, T_w is the water temperature, λ_w, Cp_w is thermal conductivity and heat capacity at constant pressure respectively.

The viscosity of droplet is much larger than that of the air, and the water film is thin, so the velocity of the water film in the normal direction is much smaller than u. The flow features of water film are similar with that of the air, so the hypothesis in the process of establishing the boundary layer equations is used:

$$u,\ v,\ \frac{\partial u}{\partial y},\ \frac{\partial u}{\partial s},\ \frac{\partial v}{\partial y},\ \frac{\partial v}{\partial s}, \tag{2.2}$$

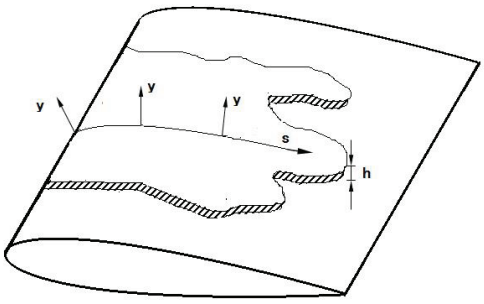


Figure 2: Coordinate system of water film flow.

https://doi.org/10.4208/aamm.2015.m1175 Published online by Cambridge University Press

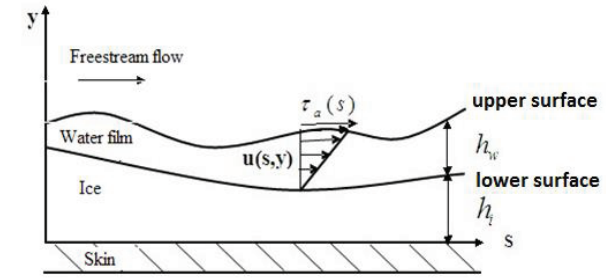


Figure 3: Water film on an iced surface.

then Eq. (2.1a) and Eq. (2.1b) can be simplified as:

$$\rho_w\frac{\partial u}{\partial t}+\rho_w\left(u\frac{\partial u}{\partial s}+v\frac{\partial u}{\partial y}\right)=-\frac{\partial p}{\partial s}+\mu\left(\frac{\partial^2 u}{\partial s^2}\right)+\rho_w g_s, \tag{2.3a}$$

$$-\frac{\partial p}{\partial y}+\rho_w g_y=0. \tag{2.3b}$$

The upper and lower surfaces of water film interface with air flow and ice layer respectively, as shown in Fig. 3, where h_i and h_w are the thickness of ice layer and water film, τ_a is the shear stress on the interface of air and water film. The following gas-liquid interface and liquid-solid interface boundary conditions are imposed.

At the gas-liquid (air-water) interface:

$$\left(\mu_w\frac{\partial u}{\partial y}\right)_{y=h_w+h_i}=\tau_a, \tag{2.4a}$$

$$p=p_a-\sigma\kappa. \tag{2.4b}$$

At the liquid-solid (water-ice) interface:

$$(u)_{y=h_i}=0. \tag{2.5}$$

Based on the fact that the thickness of the water film is less than 10^{-4} meter, and the effects of gravity, pressure and surface tension on the water film flow is very small compared to the shear forces [11], the film flow is modeled as Couette flow driven by air shear forces. Therefore, as illustrated in Fig. 2, the velocity profile in water film is approximately linear:

$$u(s,y)=\frac{y}{\mu_w}\tau_a(s). \tag{2.6}$$

The average velocity of the water film in the y direction is obtained:

$$\bar{u}(s)=\frac{1}{h_w}\int_{h_i}^{h_w+h_i}u dy=\frac{h_w}{2\mu_w}\tau_a(s). \tag{2.7}$$

https://doi.org/10.4208/aamm.2015.m1175 Published online by Cambridge University Press

The upper surface of the water film falling encounters droplets and evaporation of water. The water film starts to freeze at its lower surface gradually, which defines a free boundary problem with phase transition. The velocity of water film flowing in the direction of y is so small that the position (called the free surface) whose normal distance to the surface is equal to the height of water film is taken as the interface of water and air. The free surface can be captured by means of the height function method. In this method, the film thickness is defined as the control volume thickness, where the control volume is characterized by upper air/water interface and lower water/ice interface. Thus, by solving the film thickness h_w, the film movement can be known. Based on the theory discussed above, the film continuity equation can be derived from the mass conservation:

$$\frac{\partial}{\partial t}(\rho_w h_w)+\frac{\partial}{\partial s}\Big(\int_{h_i}^{h_w+h_i}\rho_w u dy\Big)=m_{imp}{}'-m_{evp}{}'-m_{ice}{}'. \tag{2.8}$$

By adopting Eq. (2.7), the film continuity equation in conjunction with the kinematic equations is obtained:

$$\rho_w\Big[\frac{\partial h_w}{\partial t}+\frac{\partial}{\partial s}\Big(\frac{{h_w}^2}{2\mu_w}\tau_a\Big)\Big]=V_0\cdot LWC\cdot\beta-m_{evp}{}'-m_{ice}{}'. \tag{2.9}$$

Where $m_{imp}{}'$ is the water mass of impingement, $m_{evp}{}'$ is the water mass of evaporation, $m_{ice}{}'$ is the water mass of freezing, β is the collection efficiency which is the ratio of the actual mass of collected droplets and the maximum mass of collected droplets, LWC is liquid water content (kg/m^3), V_0 is the velocity of free stream.

2.2 Water film breakdown and rivulets formation

Research showed [12] that for a thin film flowing on a vertical surface, the film will become unstable and break down as isolated rivulets if the mass flow reduces. The mechanism of film breakdown varies due to the effects of fluid property, flow conditions and boundary conditions. Three models have been proposed to determine the breakdown position. They are force balance model, minimum total energy model and surface wave disturbance model. The force balance model was established by Hartley and Murgatroyd [13] in the study of dry patches formed by isothermal film breakdown, and extended by later researchers. It estimates the critical thickness of the thin film by force balance at the breakdown position. The minimum total energy was initiated by Hobler [14] and developed by Mikielewicz and Moszynski [15,16] based on the minimum energy theory. It states that if the total energy in a given streamwise length of a liquid film or rivulet is minimum, the film or the rivulet will break down. And Joo [17], Bankoff [18] and Oron [19] analyzed the disturbance on the film surface and inside the film using long-wave theory and raised the surface wave disturbance by adopting linear theory of waves to get the breakdown condition.

For the surface wave disturbance method, when the film breakdown occurs due to the disturbance, the linear theory does not work anymore. And the effects of solid/liquid

https://doi.org/10.4208/aamm.2015.m1175 Published online by Cambridge University Press

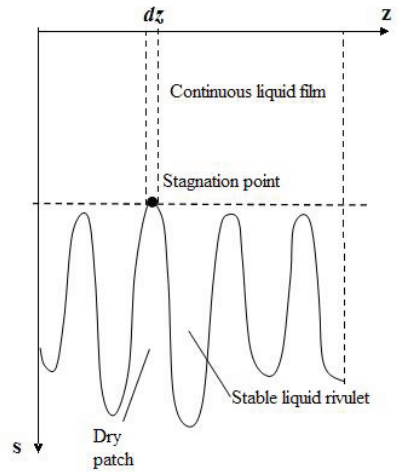


Figure 4: Rivulets and dry patches formation.

contact characteristics (generally represented by contact angle) have not been included in this model. It's pointed out [20] that the value of critical thickness derived from minimum total energy is close to that from force balance. This paper makes an analogy between the film flow over a vertical surface and over an airfoil, and determines the critical film thickness by the force balance. When the film height derived from film governing equation is less than the minimum film height, film breaks down to rivulets. And when the rivulet height derived from rivulet governing equation is less than the minimum rivulet height, rivulets break down to beads.

Considering a liquid film flowing on a vertical plate under the effects of shear stress and gravity, it's observed that if the mass flow decreases, dry patches will form and spread, and consequently the water begins to flow as rivulets. The process is shown in Fig. 4. At the stagnation point if the dry patch is stable, the surface tension must balance the gravity and fluid pressure given by the conversion of the kinetic energy of the film upstream into static pressure.

In this paper, by analogizing on a liquid film flowing on a vertical plate, water film flows on the wing surface is analyzed. The force analysis for the film breakdown position is indicated in Fig. 5.

The force exerted by the static pressure which is transformed from the upstream kinetic energy is given as:

$$F_p = dz \int_0^{h_w} \frac{1}{2} \rho_w u^2(s,y) dy. \tag{2.10}$$

The surface tension opposes this force:

$$F_{\sigma 2} = F_{\sigma 1} = \sigma dz. \tag{2.11}$$

https://doi.org/10.4208/aamm.2015.m1175 Published online by Cambridge University Press

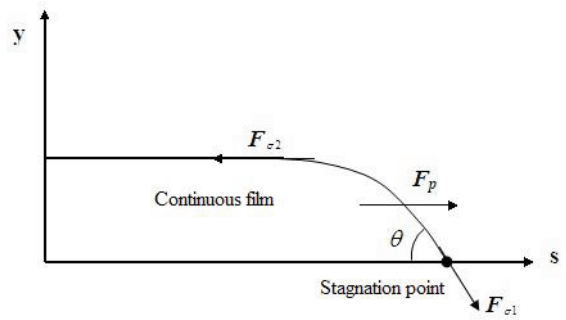


Figure 5: Force balance at the breakdown position.

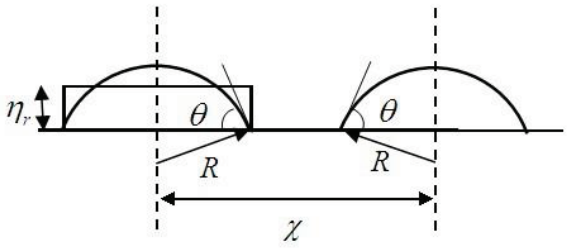


Figure 6: Cylindrical rivulet cross section.

Where, σ is the surface tension coefficient.

Thus, equating the pressure force to the horizontal component of the surface tension, one can get the minimum film height where the film breaks down to rivulets:

$$F_{\sigma 2} - F_{\sigma 1}\cos\theta = F_p, \tag{2.12a}$$

$$h_{f-r} = \left[\frac{6\cdot {\mu_w}^2\cdot\sigma\cdot(1-\cos\theta)}{\rho_w {\tau_a}^2}\right]^{1/3}. \tag{2.12b}$$

Where both of θ and σ are functions of surface temperature t_f. In the calculation, they are determined by the surface temperature according to the fitting curve of experimental data from [21,22]. And the expressions are as follows:

$$\theta = -370.3849 + 379.4328\times 10^{-0.0042 t_f} - 2.2962\times 10^{24.1087 t_f}, \tag{2.13a}$$

$$\sigma = 0.07564 - 0.00014 t_f. \tag{2.13b}$$

Suppose that rivulets are uniformly distributed in spanwise direction. Define center-to-center rivulets spacing χ and rivulet radius R, as shown in Fig. 6.

From rivulet geometry presented above, the rivulet wetness factor F_r is given by:

$$F_r = \frac{2R\sin\theta}{\chi}. \tag{2.14}$$

https://doi.org/10.4208/aamm.2015.m1175 Published online by Cambridge University Press

With the assumption of Couette flow, the mass flow rate of water film m_f and rivulet m_r can be described [15]:

$$\dot{m}_f = \int_{h_i}^{h_w+h_i} \rho_w u(s,y)dy = \frac{\rho_w \tau_a}{2\mu_w} {h_w}^2, \tag{2.15a}$$

$$\dot{m}_r = \frac{2}{\chi} \int_0^{R\sin\theta} \int_{h_i}^{h(s)+h_i} \rho_w u(s,y)dsdy = \frac{\rho_w \tau_a}{\mu_w} \frac{\phi(\theta)}{\chi} R^3. \tag{2.15b}$$

Then the total mechanical energy of film e_f and rivulet e_r can be approximately estimated by:

$$e_f = \int_{h_i}^{h_w+h_i} \frac{\rho_w}{2} u^2(s,y)dy + \sigma_{lv} + \sigma_{ls} = \frac{\rho_w {\tau_a}^2}{6{\mu_w}^2} {h_w}^3 + \sigma_{lv} + \sigma_{ls}, \tag{2.16a}$$

$$\begin{aligned} e_r &= \frac{\rho_w}{\chi} \int_0^{R\sin\theta} \int_{h_i}^{h(s)+h_i} u(s,y)dsdy + \left(\frac{2R\theta}{\chi} + \cos\theta - \frac{R\sin 2\theta}{\chi}\right) + \sigma_{lv} + \sigma_{ls} \\ &= \frac{\rho_w {\tau_a}^2}{6{\mu_w}^2} g(\theta) {h_w}^3 \left[\frac{\sin\theta}{\phi(\theta)}\right]^{\frac{3}{2}} + \left(F_r \frac{\theta}{\sin\theta} + \cos\theta - F_r \cos\theta\right)\sigma_{lv} + \sigma_{ls}. \end{aligned} \tag{2.16b}$$

At the breakdown position, the mass and total mechanical energy conservation is applied to the transition from film flow to rivulet pattern, i.e., Eq. (2.15a) equals to Eq. (2.15b), and Eq. (2.16a) equals to Eq. (2.16b). Since the rivulet initial thickness is already known as the minimum film height solved using Eq. (2.12b), the geometrical parameters R, F_r and χ in the break-down position can be derived from Eq. (2.15a) to Eq. (2.16b). χ is assumed to be constant when rivulets flow downstream.

After the calculation of the rivulet flow pattern parameters (R, F_r and χ), N-S equations for one single rivulet can be established. Similar to the development process of the water film continuity equation, the continuity equation for one single rivulet can be obtained using height function method to capture the free surface and Couette assumption to describe velocity profile:

$$\rho_w \left[\frac{\partial A_r}{\partial t} + \frac{\partial}{\partial s}\left(\frac{\dot{m}_r}{1/\chi}\right)\right] = \delta \cdot V_0 \cdot LWC \cdot \beta - \delta \cdot {m_{evp}}' - \xi \cdot {m_{ice}}'. \tag{2.17}$$

2.3 Rivulets breakdown and beads formation

When rivulet mass flow keeps reducing, rivulets may break down as isolated beads. The critical rivulet thickness at the breakdown position is also obtained from the force balance. The external forces acting on a bead are the gravitational force (F_g), the shear stress exerted by the airfoil (F_d), and the pressure gradient along the profile (p). The bead's surface tension (F'_σ) will resist movement. Fig. 7 presents the forces and the bead parameters.

Hence, these four forces in the chord-wise direction s:

$$F_{ds} + F_{gs} + F_{\mathrm{ps}} = F_{\sigma s}. \tag{2.18}$$

https://doi.org/10.4208/aamm.2015.m1175 Published online by Cambridge University Press

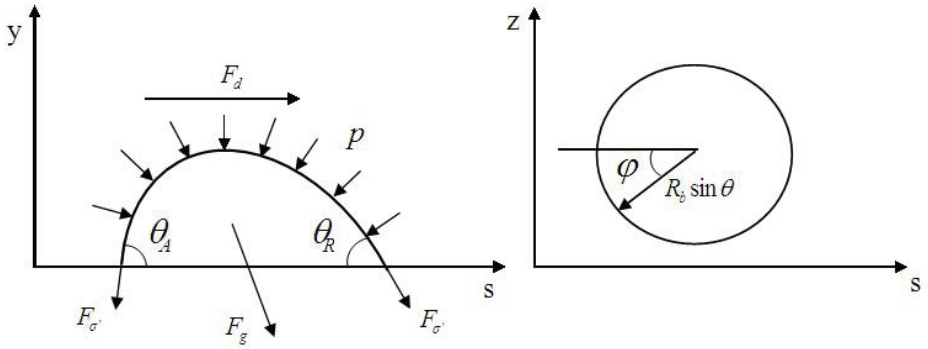


Figure 7: Deformed bead, forces and relevant angles.

By integrating the projection of the surface tension along the contact line, the surface tension is found:

$$F_{\sigma s}=2\int_0^{\pi}\sigma\cos(\theta(\varphi))R_b\cos\varphi d\varphi=\frac{24}{\pi^3}\sigma(\cos\theta_A-\cos\theta_R)h_b\frac{\sin\theta}{1-\cos\theta}. \tag{2.19}$$

The shear stress exerted by the airfoil as a function of the bead height is defined as:

$$F_{ds}=\tau_a\cdot\pi\frac{\sin^2\theta}{(1-\cos\theta)^2}{h_b}^2. \tag{2.20}$$

The pressure gradient force:

$$F_{ps}=2\pi\frac{\partial p}{\partial s}\frac{\sin\theta}{(1-\cos\theta)}{h_b}^2. \tag{2.21}$$

The gravitational force:

$$F_{gs}=\pi\frac{(\frac{2}{3}-\cos\theta+\frac{1}{3}\cos^3\theta)}{(1-\cos\theta)^3}\rho_w{h_b}^3 g_s. \tag{2.22}$$

Where θ_A and θ_R can be calculated by the fitting curve derived from the experimental data in [25,26]. And the expressions are as follows:

$$\Delta\theta=\theta_A-\theta_R=896.7028\times10^{-0.8233t_f}+5.7021\times10^{-0.0823t_f}-902.3850\times10^{0.8397t_f}, \tag{2.23a}$$

$$\theta_R=0.8333\theta_A+5.0. \tag{2.23b}$$

Thus by solving Eq. (2.18), the bead maximum height h_b can be found, and the minimum rivulet height h_{r_b} is the product of h_b and the shape factor f_s

$$h_{r_b}=f_s\cdot h_b,\quad f_s=\frac{\theta-\sin\theta\cos\theta}{2\sin\theta}. \tag{2.24}$$

https://doi.org/10.4208/aamm.2015.m1175 Published online by Cambridge University Press

Within the beads area, the water is relatively stable and runback does not occur [6]. The size and distribution of beads is rather random. To simplify the calculation, beads are considered to reach thermodynamic equilibrium in a very short time. Thus, the mass and energy balance in beads area states that:

$$m_{imp}{}' - m_{remain}{}' - m_{evp}{}' - m_{ice}{}' = 0, \tag{2.25a}$$

$$q_{imp} - q_{evp} - q_{conv} - q_{remain} - q_{ice} = 0. \tag{2.25b}$$

3 Multi-zone roughness model

Experiments show that an iced surface is not smooth, and is a collection of small and nearly hemispherical caps with radii of the order of millimeters [23]. Since roughness is induced by the ice accretion, it varies with time and space. The roughness shape and distribution are intuitively related to the size and evolution of the rivulets and beads formed on the surface, and their interaction with the accreted layer. Surface roughness will affect the behavior of the boundary layer in terms of heat transfer and shear stress [24]. On the other hand, both shear stress and heat transfer determine the shape and size of the accreted ice layer. Therefore there is an unsteady coupling between roughness build-up and ice accretion.

Most icing codes provide rather simplified roughness model through the use of empirical correlations. The most widely employed correlation was proposed by Shin and Bond [25], giving a single, average, representative value of roughness as a function of cloud liquid water content (LWC), droplet mean volumetric diameter (MVD), ambient temperature and aircraft speed. Thus, in the whole ice accretion process the roughness value is assumed to be constant in time and space which does not agree with the real roughness evolution discussed above.

Therefore, a more accurate roughness model is needed. In this paper, an analytical model to calculate the surface roughness in the wet regime based on three liquid water states on an airfoil surface: continuous film, rivulets and beads is adopted.

3.1 Continuous film

Film height h_w is calculated by performing a mass balance over the control volume, i.e., Eq. (2.12a). When h_w is greater than the minimum film height h_{f-r}, the surface water forms a film, and the roughness height is considered to be equal to the wave height over the film [26]:

$$k_s = 0.75 \cdot \frac{\tau_a}{\mu_w} \cdot \sqrt{\frac{{h_w}^3}{g}}. \tag{3.1}$$

https://doi.org/10.4208/aamm.2015.m1175 Published online by Cambridge University Press

3.2 Rivulets

When film height h_w is less than the minimum film height h_{f-r}, the water on the surface forms rivulets, and the roughness height is considered to be equal to the local rivulet height:

$$k_s = h_r. \tag{3.2}$$

3.3 Beads

When film height h_w is less than the minimum rivulet height h_{r-b}, the water on the surface forms beads, and the roughness height is considered to be equal to the height that bead reaches before moving:

$$k_s = h_b. \tag{3.3}$$

4 The heat transfer in layers and on the water/ ice interface

4.1 Water layer

Simplifying the film energy Eq. (2.1a) under general icing conditions through magnitude analysis leads to:

$$\frac{\partial}{\partial y}\left(\lambda_w \frac{\partial T_w}{\partial y}\right) = 0. \tag{4.1}$$

The temperature profile in water film is approximately linear.

To simplify rivulet energy equation, rivulets are equivalent to a rectangle flow with the same cross sectional area and the same bottom edge.

4.2 Ice layer

Through the magnitude analysis, we can also get the simplified energy equation in ice layer:

$$\frac{\partial}{\partial x_j}\left(\lambda_i \frac{\partial T_i}{\partial x_j}\right) = 0. \tag{4.2}$$

In the case that ice accretes on airfoil without anti-ice system installed, the skin is considered to be adiabatic and the temperature at water/ice interface is the phase-transition temperature:

$$T_i(y) \equiv T_m, \tag{4.3a}$$

$$\left(\lambda_i \frac{\partial T_i}{\partial y}\right)_{y=0} = 0. \tag{4.3b}$$

https://doi.org/10.4208/aamm.2015.m1175 Published online by Cambridge University Press

Solving Eq. (4.2) by applying the boundary conditions Eqs. (4.3a) and (4.3b), one can get the temperature profile of the ice layer:

$$T_i(y) \equiv T_m. \tag{4.4}$$

4.3 Water/ ice interface

Stefan condition is applied at the water/ice interface:

$$m_{ice}{}' \cdot L_f = -\lambda_w \frac{\partial T_w}{\partial y} + \lambda_i \frac{\partial T_i}{\partial y}, \tag{4.5}$$

where $m_{ice}{}'$ is freezing mass flux, equal to $\rho_i \frac{\partial h_i}{\partial t}$. By substitution of Eqs. (4.1) and (4.4) to Eq. (4.5), one obtains:

$$\rho_i L_f \frac{\partial h_i}{\partial t} = \lambda_w \frac{T_m - T_f}{h_w}, \tag{4.6}$$

where T_f is the surface temperature of film.

At the water/air interface as shown in Fig. 8, according to the energy balance there is:

$$q_{cond} = (q_{conv} + q_{evp} + q_{rad} + q_{war}) - (q_{air} + q_{kin} + q_{fre}). \tag{4.7}$$

Where the heat flux presented above are:

(1) Conductive heat transfer in the film q_{cond}, and

$$q_{cond} = \left(-\lambda_w \frac{\partial T_w}{\partial y} \right)_{y=h_w}. \tag{4.8}$$

(2) Convective heat transfer at the water surface q_{conv}.

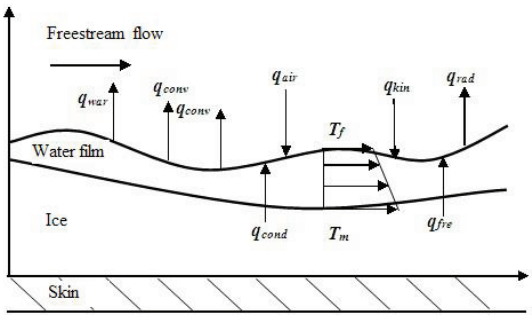


Figure 8: Energy balance for water film.

https://doi.org/10.4208/aamm.2015.m1175 Published online by Cambridge University Press

(3) Aerodynamic heating q_{air}, and

$$q_{conv}-q_{air}=htc(T_w-T_{rec}). \tag{4.9}$$

(4) Radiative heat transfer q_{rad}

$$q_{rad}=\sigma_r({T_w}^4-{T_0}^4). \tag{4.10}$$

(5) Cooling by incoming droplets q_{war}.

(6) Kinetic energy of incoming droplets q_{kin}, and

$$\begin{aligned} q_{war}-q_{kin}&={m_{imp}}'\cdot\left[c_{pw}(T_w-T_d)-\frac{\|u_d\|^2}{2}\right]\\ &=V_0\cdot LWC\cdot\beta\cdot\left[c_{pw}(T_w-T_d)-\frac{\|u_d\|^2}{2}\right]. \end{aligned} \tag{4.11}$$

(7) Evaporative heat transfer q_{evp}, and for glaze ice (with liquid water existing on the surface):

$$q_{evp}={m_{evp}}'\cdot L_e \tag{4.12}$$

for rime ice (without liquid water on the surface):

$$q_{evp}={m_{evp}}'\cdot L_f. \tag{4.13}$$

(8) Release of latent heat by freezing q_{fre}, and

$$q_{fre}={m_{imp}}'\cdot L_f=V_0\cdot LWC\cdot\beta\cdot L_f. \tag{4.14}$$

5 Solution of governing equations

Water film flowing on the surface is driven by several forces emerges a movement forefront issue. At the forefront of film movement, large curvature would arise in some cases which should be considered. To properly solve this problem, referring to the research of film flow driven by gravity [11], it is assumed that a very thin film is existed on the surface at the initial time.

The method for solving an ice accretion problem proceeds is as following:

(1) Calculate T_w iteratively and gain the freezing mass flux at that moment by substitute known film thickness h_w and Eq. (4.6) to Eq. (4.7).

(2) With T_w already known, calculate every term on the right-hand side of Eq. (2.9).

(3) For the left-hand side of Eq. (2.9), solve the space derivative term via central difference method and determine h_w at next moment through Runge-Kutta method.

https://doi.org/10.4208/aamm.2015.m1175 Published online by Cambridge University Press

(4) Repeat Step 1 to 3 until the film is stable. Estimate the film breakup position and conduct rivulets calculation. Based on the results of rivulet calculation, the rivulet breakup position and conduct beads are calculated. Update surface roughness via Eqs. (3.1)-(3.3).

(5) Calculate the freezing mass flux in the steady state with new surface roughness via Eq. (4.6).

(6) Sum the freezing mass flux in each moment to get the total freezing mass.

Obviously, an unsteady icing process can be solved by the method presented above.

6 Results and discussion

6.1 Test cases

Ice accretion on a NACA0012 airfoil is simulated under the conditions shown in Table 1. The total simulation time is 6 minutes. The flow field and water droplet trajectories are updated every 60s. Ice shapes obtained at the end of the simulation are compared to those obtained experimentally in the NASA Lewis Icing Research Tunnel [27] under the same condition.

6.2 Film thickness

Fig. 9 shows the film height h_w (without breakup) distribution with the change of the surface distance (s/m) at four temperatures (-2.2°C, -3.9°C, -7.8°C and -26.1°C, denoted as Case 1, Case 2, Case 3 and Case 4, respectively). Film height reduces along with the decreased temperature which corresponds to the tendency of ice shapes from glaze ice to rime ice. When the temperature is relatively high, water film appears on the surface, and the height of the film varies at locations. While at -26.1°C, a low temperature, film barely exists and rime ice is formed on the surface.

Many widely used models like Messinger Ice Accretion Model assume that the water film distributes uniformly on the airfoil surface. Some models even do not consider the existence of the water film when simulating the icing accretion. Our simulation shows that these assumptions are not realistic, especially when the meteorological temperature

Table 1: Conditions of numerical simulation.

Chord	0.5334m
Angle of attack	4°
Mach number	0.197
Atmospheric pressure	101300Pa
Liquid water content	1.0g/m^3
Median volumetric diameter	20.0mm
Accretion time	360s

https://doi.org/10.4208/aamm.2015.m1175 Published online by Cambridge University Press

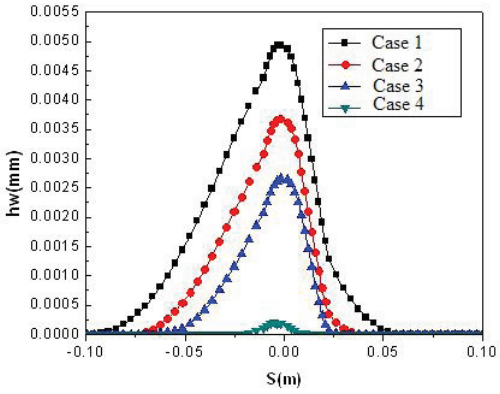


Figure 9: Film height before breakdown on NACA0012 airfoil.

is relatively high. Movement of water film on the airfoil surface should be considered to improve accuracy of model prediction of the liquid mass distribution, impact range and the local collection efficiency.

6.3 Roughness height

Figs. 10-13 show the roughness height distribution with the change of the surface distance (s/m) which is calculated at the four temperatures (-4.4°C, -6.1°C, -10.1°C and -28.3°C), respectively. At higher temperatures (-4.4°C and -6.1°C), water on the upper surface flows to the next control volume and form a liquid film. In these high temperature (-4.4°C and -6.1°C) cases, the roughness height is at a minimum at the stagnation point. Along the stream-wise direction, due to film breakdown, roughness increases rapidly and reaches a maximum, after which it decreases towards the ice end. For lower temperature

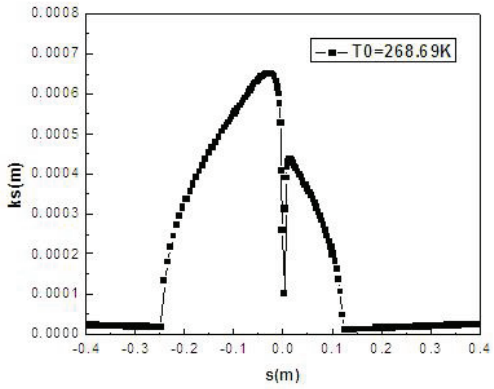


Figure 10: Roughness distribution at -4.4°C.

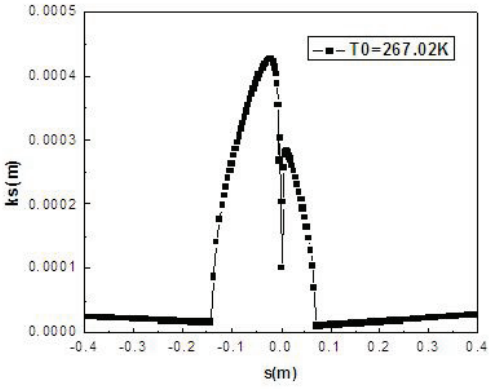


Figure 11: Roughness distribution at -6.1°C.

https://doi.org/10.4208/aamm.2015.m1175 Published online by Cambridge University Press

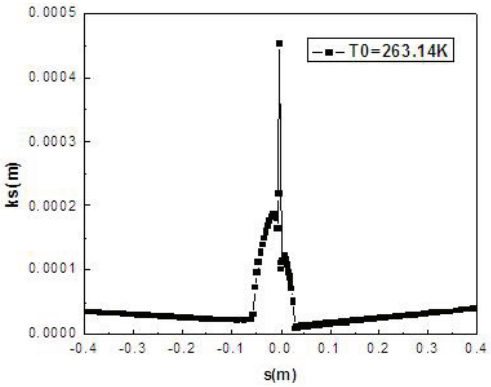


Figure 12: Roughness distribution at -10.1°C.

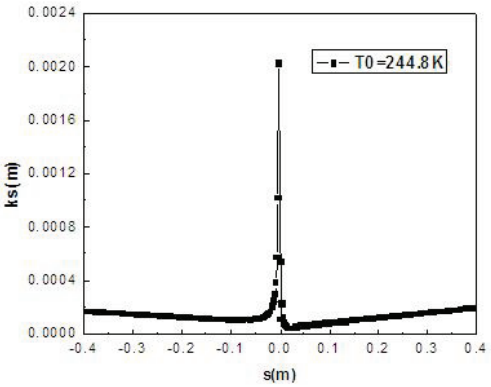


Figure 13: Roughness distribution at -28.3°C.

(-28.3°C), super-cooled water droplets freeze on impact and form beads. The beads result in surface roughness. The roughness height is at a maximum at the stagnation point and decreases towards the ice end.

It can be seen that roughness height varies with respect to location. Assuming that the roughness is constant and uniform distribution on the airfoil surface will cause a big discrepancy between parameter values characterizing icing on the airfoil surface obtained by simulations and those measured experimentally.

6.4 Ice accretion shapes

Figs. 14-17 show comparison between shapes of the ice predicted using the present icing and roughness model and those measured experimentally, and those predicted by LEWICE. The ice mass distribution, freezing limitation, horns of ice, ice shape predicted by the present model is in better agreement with the experimental data. So the consideration for exiting of water film and the evolution process are very important for establishing the ice accretion model, which is more complying with the real physical process as shown in this paper. But the freezing limits on upper and lower surfaces at warm temperatures are bigger than those measured, as well as those predicted by LEWICE, which may be caused by the inaccurate assumption in 2D situations that water flows to the next downstream volume. At cold temperatures, water mostly freezes as soon as impact, therefore the freezing limits on upper and lower surfaces are very close to the experimental data as well as LEWICE. The simulation presents the tendency from glaze ice formation to rime ice formation due to the decreased temperature. So in these rime ice formation conditions, both the multi-zone ice accretion model and the Messinger icing model may predict very well. When temperature increases, such as at -3.9°C, as shown in Fig. 14, because the relatively high temperature, water collected on the surface will not freezing immediately, and will flow downstream in the direction of chord, so the freezing limitation will be wider than the droplet impact limitation. In this case, ice freezing mass

https://doi.org/10.4208/aamm.2015.m1175 Published online by Cambridge University Press

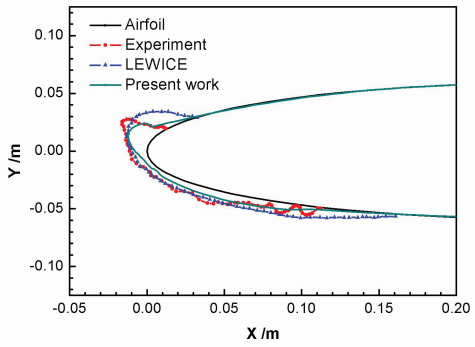


Figure 14: Ice shape of Case 1.

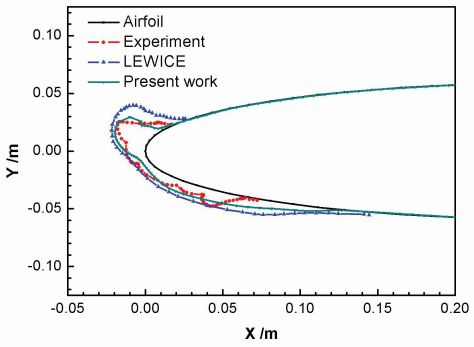


Figure 15: Ice shape of Case 2.

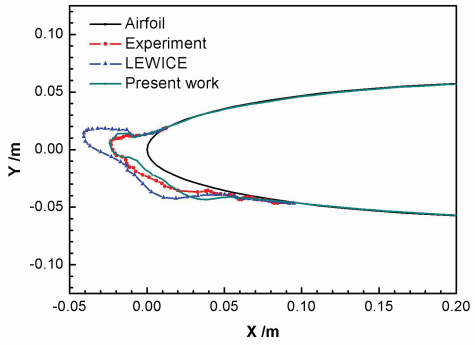


Figure 16: Ice shape of Case 3.

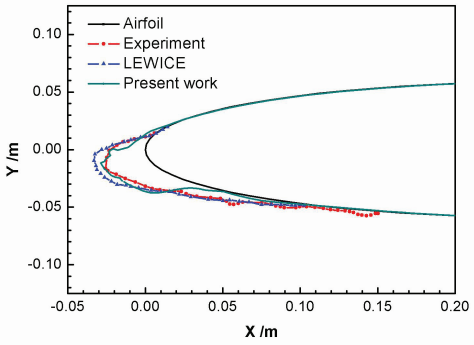


Figure 17: Ice shape of Case 4.

distribution, limitation, and shape is more consistent with the experiment results, as the process of water flow and roughness formation are considered in the new icing model presented in this paper.

7 Conclusions

In this article, a multi-zone icing model and the corresponding roughness model were developed considering water film breakup, rivulets and beads formation. Ice accretion on NACA0012 airfoil was simulated by using the new model. Simulation results are shown to be agreed well with the tunnel experimental results. The model simulation reveals that when droplet impinges the airfoil surface, water film is formed and flows downstream, and then evolves into rivulets and beads. This phenomenon in the relatively high temperature conditions is particularly evident. Change of the liquid flow form on the surface altered the surface roughness, resulting in roughness varying with time and surface locations. Therefore it is suggested that the formation and development of water film and roughness on the surface cannot be ignored in aircraft icing simulation, especially for glaze ice conditions.

https://doi.org/10.4208/aamm.2015.m1175 Published online by Cambridge University Press

Acknowledgments

This work is supported by the "Fundamental Research Funds for Central Universities", Nanjing University of Aeronautics and Astronautics Basic Scientific Research Projects for Youth Science (No. NS2014014).

References

[1] COLIN S. BIDWELL AND MARK G. POTAPCZUK, *Users manual for the NASA Lewis three-dimensional ice accretion code (LEWICE3D),* NASA Technical Memorandum, (1993), 105974.
[2] T. HEDDE AND D. GUFFOND, *Onera three-dimensional icing model,* AIAA J., 33(6) (1995), pp. 1038–1044.
[3] W. B. WRIGHT, G. W. GENT AND D. GUFFOND, *DRA/NASA/ONERA collaboration on icing research part II-prediction of airfoil ice accretion,* NASACR-202349, 1997.
[4] V. MINGIONE AND BRANDI B. ESPOSITO, *Ice Accretion predict on multi-element airfoils*, AIAA-97-0177, 1997.
[5] H. BEAUGENDRE, F. MORENCY AND W. G. HABASHI, *FENSAP-ICE: roughness effects on ice shape prediction,* AIAA-2003-1222, 2003.
[6] R. J. HANSMAN AND S. R. TURNOCK, *Investigation of surface water behavior during glace ice accretion,* AIAA-88-0015, 1988.
[7] R. J. HANSMAN, K. YAMAGUCHI, B. BERKOWITZ AND M. POTAPCZUK, *Modeling of surface roughness effects on glaze ice accretion,* AIAA-89-0734.
[8] K. YAMAGUCHI, R. J. HANSMAN AND B. BERKOWITZ, *Deterministic multi-zone ice accretion modeling,* AIAA-91-0265.
[9] J. SHIN, *Characteristics of surface roughness associated with leading edge ice accretion,* AIAA-94-0799, 1994.
[10] Y. BOURGAULT, W. G. HABASHI AND H. BEAUGENDRE, *Development of a shallow water icing model in FENSAP-ICE,* AIAA-99-0246, 1999.
[11] S. P. OTTA AND A. P. ROTHMAYER, *A simple boundary-layer water film model for aircraft icing,* AIAA-2007-902.
[12] XUEMIN YE, JUNGANG YAN, CHUNXI LI AND WEIPING YAN, *Breakdown model of locally heated and subcooled films driving by interfacial shear and gravity,* Journal of North China Electric Power University, 37(2) (2010), pp. 63–68.
[13] D. E. HARTLEY AND W. MURGATROYD, *Criteria for the break-up of thin liquid layers flowing isothermally over solid surfaces,* Int. J. Heat Mass Transfer, 7(7) (1964), pp. 1003–1015.
[14] T. HOBLER, *Minimal surface wetting,* Chemia Stosow, 2B(201) (1965).
[15] J. MIKIELEWICZ AND J. R. MOSZYNSKI, *Breakdown of a shear driven liquid film,* Trans. IFFM, 66 (1975), pp. 3–11.
[16] J. MIKIELEWICZ AND J. R. MOSZYNSKL, *Minimum thickness of a liquid film flowing vertically down a solid surface,* Int. J. Heat Mass Transfer, 19(7) (1976), pp. 771–776.
[17] S. W. JOO, S. H. DAVIS AND S. G. BANKOFF, *Long-wave instabilities of heated falling films: two-dimensional theory of uniform layers,* J. Fluid Mech., 230 (1991), pp. 117–146.
[18] S. G. BANKOFF, *Significant questions in thin liquid film heat transfer,* Trans. ASME. J. Heat Transfer, 116(1) (1994), pp. 10–16.
[19] A. ORON, S. H. DAVIS AND S. G. BANKOFF, *Long-scale evolution of thin liquid films,* Rev. Modern Phys., 69(3) (1997), pp. 931–980.

https://doi.org/10.4208/aamm.2015.m1175 Published online by Cambridge University Press

[20] D. E. HARTLEY AND W. MURGATROYD, *Criteria For the break-up of thin liquid layers flowing isothermally over solid surfaces,* Int. J. Heat Mass Transfer, 7(7) (1964), pp. 1003–1015.
[21] R. J. HANSMAN JR, A. REEHORST AND J. SIMS, *Analysis of surface roughness generation in aircraft ice accretion,* AIAA-92-0298, 1992.
[22] G. LUXFORD, *Experimental and modeling investigation of the deformation, drag and break-up of drizzle droplets subjected to strong aerodynamics forces in relation to SLD aircraft icing,* Cranfield University School of Engineering, 2005.
[23] D. N. ANDERSON, D. B. HENTSCHEL AND G. A. RUFF, *Measurement and correlation of ice accretion roughness,* AIAA-98-048, 1998.
[24] M. B. BRAGG, M. KERHO AND J. WINKLER, *Effects of initial ice roughness on airfoil aerodynamics,* AIAA-94-0800, 1994.
[25] J. SHIN, B. BERKOWITZ, H. H. CHEN AND T. CEBECI, *Prediction of ice shape and their effect on airfoil performance,* AIAA-91-0264, 1991.
[26] P. M. GERHART, R. J. GROSS AND J. I. HOCHSTEIN, Fundamentals of Fluid Mechanics, Second Edition, Addison-Wesley Publishing Company, 1992.
[27] H. H. CHEN AND T. CEBECI, *A turbulence model for iced airfoils and its validation,* AIAA-92-0417, 1992.

https://doi.org/10.4208/aamm.2015.m1175 Published online by Cambridge University Press